

# Millimeter-Wave Tightly-Coupled Phased Array with Integrated MEMS Phase Shifters

Anas J. Abumunshar<sup>1, \*</sup>, Kubilay Sertel<sup>2</sup>, and Niru K. Nahar<sup>2</sup>

**Abstract**—A low-loss electronic beam steering model is presented in this paper based on tightly-coupled dipole array topology for satellite communications applications for K through Ka-band (18–40) GHz. The array is low-profile having  $< 3.4$  mm height and printed on an affordable single-layered PCB. As proof-of-concept, a  $4 \times 4$ -element, single polarized array is fabricated and measured showing (18–40) GHz (VSWR  $< 2$ ) continual band coverage. A compact, low-loss electronic beam steering architecture for moderate bandwidth arrays is also utilized for beam steering. A 2-bits tunable phase shifter, spanning over (18–30) GHz with  $IL < 2.5$  dB, is developed using micro-electro mechanical systems (MEMS) technology. The phase shifter is integrated with the array elements resulting in reduced size, cost, and complexity of the feeding network. A full-wave simulation of the  $4 \times$  Infinite array with the integrated MEMS phase shifter is conducted to prove the concept.

## 1. INTRODUCTION

This paper is the extension of the work originally presented in [1, 2]. The growing need for cellular and personal communications services (PCS), and the increasing demand for exchanging high-resolution video and other types of data in commercial and military applications continue to fuel research for higher-bandwidth, conformal, and more agile radiators and front ends [3]. The current military systems typically consist of common sets of broadband apertures that replace most of the antennas and RF sensors installed in a platform [4, 5]. However, smaller and more agile missiles operating in non-conventional warfare require faster scanning speeds. Unmanned aerial vehicles (UAVs), as illustrated in Fig. 1, and fast moving tactical missiles require fast scanning and rapid scene correlation to deliver early warning of attack. Specifically, higher Ka-bands for SATCOM and 5G commercial applications are current areas of research to fulfill the ever-increasing connectivity needs of the society [6]. Yet, developing the next generation of wireless systems at Ka-band that can keep pace with the high-performance of SATCOM applications is a challenging goal. Mobile platforms such as wireless sensors, unmanned vehicles, or hand-held devices have limited size, weight, and specific power budget. Additionally, the distribution of these functionalities across large number of devices and users require low-cost implementation.

Current beam steering technologies in the Ka-band include hybrid mechanical-electrical beam scanning [7], switched beam array [8], microfluidic based antenna [9], and reflect array antenna technology [10]. However, these technologies are narrowband, bulky, heavy, and convey mechanical movements that interfere with the vehicle's aerodynamics. To address these issues, electronic scanning antennas (ESAs) that enable rapid beam pointing without mechanical manipulation can be utilized. Consequently, wideband ESAs with low physical profile, as well as simple, and cost-effective fabrication method for the next generation of SATCOM applications at Ka-band are being developed. Of particular interest is wideband low-profile phased array that can electronically steer their beam and cover wide

---

Received 30 November 2020, Accepted 18 February 2021, Scheduled 23 February 2021

\* Corresponding author: Anas J. Abumunshar (anas.abumunshar@intel.com).

<sup>1</sup> Intel Corporation, USA. <sup>2</sup> The ElectroScience Laboratory at The Ohio State University, USA.

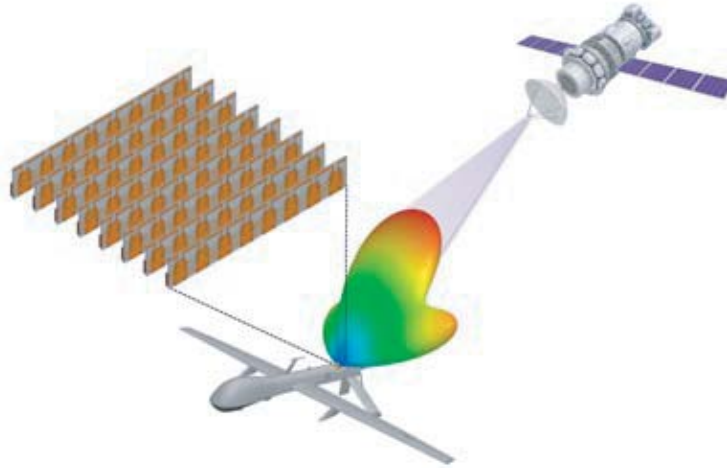


**Figure 1.** Electronic scanning array installed on an unmanned vehicle to provide beam agility of the SATCOM applications.

scanning field of view ( $\pm 45^\circ$ ). These include Tightly coupled dipole arrays (TCDA) [11–14] which are extremely low-profile while concurrently exhibiting continuous coverage of the L- through C-bands using a single aperture [15]. However, most of the existing researches focus on the antenna array design only, without mentioning the feeding network. The feeding network is vital as its complexity and loss can pose significant issue on the TCDA, especially at the higher frequency Ka-band. To address this, the antenna unit cell of the TCDA can be merged with the Marchand-balun [15]. The antenna unit cell and Marchand-balun can also be co-designed together to improve the impedance matching and increase the operational bandwidth.

In this paper, the full design of the TCDA including the feeding network is presented for the first time. The TCDA with coverage of 18–40 GHz is based from [15]. Emerging challenges in previous designs are addressed by utilizing a low-loss, compact feeding architecture ideal for moderate bandwidth large arrays. Furthermore, a low-loss ( $IL < 2.5$  dB) and compact micro-electromechanical systems (MEMS) based phase shifter that can be seamlessly integrated with the feeding network is also developed. The antenna array and feeding network are also integrated and co-designed together to improve the impedance matching and operational bandwidth. An accurate circuit model for the entire co-design using extensive parametric analysis, which can reduce time and cost of TCDA design in the future, is also developed. As proof-of-concept, a  $4 \times 4$  prototype is fabricated and tested at broad side. In addition, a full-wave simulated performance of the beam forming network is demonstrated over 18–30 GHz.

## 2. COMPACT, LOW-LOSS BEAM STEERING USING MEMS TECHNOLOGY

Currently, electronic scanning phased arrays suffer from complexity, high loss, and large weight of the corporate feeding network. These issues become more aggravated as frequency increases. On the other hand, digital beam forming networks are simple, low-loss, and low-profile. However, they are limited to narrow band applications. Therefore, there is still significant interest in simple, low-loss RF beam formers especially for wide band applications [16]. Yet, the complexity, bulkiness, and high loss of RF beam formers need to be improved. In this section, the feeding architecture and device technology as key solutions to remedy discrepancies of the RF feeding network is proposed, especially the complexity and loss.

RF beam formers owe their beam steering from the true time delay units (TDUs) and phase shifters. These units create the desired phase delays at the unit cells, leading to the beam formation. TDUs provide a constant phase delay over a wide range of frequencies contrary to phase shifters, which result in accurate beam steering and negligible squint in the beam direction. However, TDUs are bulky and have considerable losses. Wideband arrays with TDU module behind each unit cell suffer from complexity,

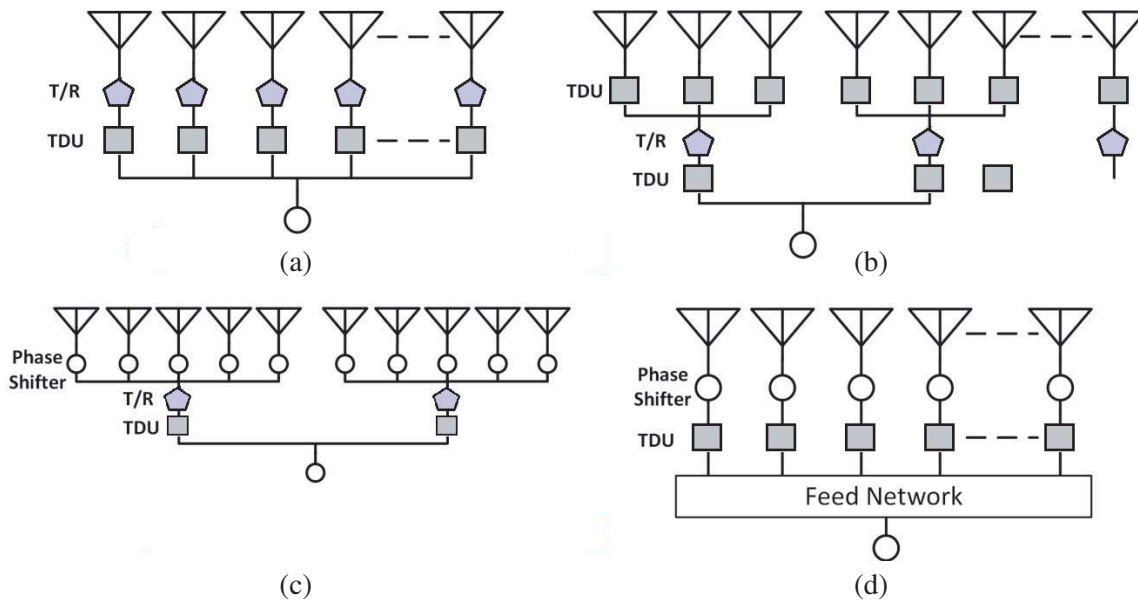


**Figure 2.** Phase shifters RF beam steering architectures.

bulkiness and huge losses.

In Fig. 2, different architectures of RF beam scanning are presented. In architecture (a), T/R module and a TDU are used per each element to provide very accurate time delay and bandwidth. The TDU loss is compensated through amplification on each element. For very large wideband arrays, this technique requires time delay by the last unit that exceeds hundreds of wavelengths, resulting in large, lossy and heavy TDU. In addition, there is little room behind each element to include the TDU and amplification. Therefore, this architecture is practical only for relatively small, wideband array. A more practical architecture is shown in (b) wherein a small increment of time delay is provided on each element, up to three wavelengths. It is characterized by longer delays at different sub-arraying levels owing to the amplification of the elements grouped into subarrays. In addition, wide scan can be provided for very long wideband arrays. The architecture in (c) is more practical for large arrays with modest instantaneous bandwidth. It consists of a phase shifter at the element level, with several elements divided into sub arrays where TDU is utilized. This architecture is simple, easy to implement, and provides room for inclusion of TDU at subarray level. Lastly, scanning of time delay beam position architecture is shown in (d), which provides time delay of small magnitude, at two to four, of beam positions. The scan sector is centered on a specific number of true-time delay positions. The phase shifters are then used to scan the beam from the time-delay position halfway to the next one. Consequently, this architecture is suitable for wideband arrays. However, the required different sets of switch lines per array element is quite costly. Hence, architecture in (c) is optimal for the 18–40 GHz TCDA design by providing continuous beam coverage for a wide angle of scanning. It also offers the capability to integrate the phase shifter at the back side of the array unit cell, thereby reducing the loss, size and complexity of the feeding network.

Phase shifters, shown in Fig. 2, can be built using Micro-Electro Mechanical System (MEMS) technology that can add attractive features to the devices at millimeter wave. MEMS technology in phase shifters is preferable over semiconductor-based phase shifters such as GaAs-based FETs, PHEMT or PIN-diode due to their small size and weight, low cost, low insertion loss (0.1 dB), good power handling abilities, low power consumption (10–100 nJ/cycle), wide bandwidth, and high isolation ( $< -30$  dB) [17–19]. They have been also utilized in phase array antennas at Ka-band to develop low-cost active seekers, and adaptive beam formers for several applications such as UAVs' sensor multi-functional radar systems and rapid beam steering for missile seekers [20]. However, MEMS suffers from low switching time, which only ranges from 1–30  $\mu$ s.

The proposed phase shifter design is built using the low-loss switched network based on MEMS

technology. This phase shifter is planar to allow seamless integration at the back side of the antenna unit cell, as described in Section 5. The feeding network and antenna are co-designed and tuned to give the optimum performance, reduced power loss and complexity of the feeding network.

### 3. K-KA BAND COUPLED DIPOLE ARRAY DESIGN

Phased arrays offer electronic steering and beam agility at low-profile, which are highly desired in SATCOM and mobile applications. Tightly Coupled Array (TCA) led to unprecedented low profile and ultra-wide bandwidth and was used in RF frequency bands, such as those outlined in [15, 21–24]. The unit cell can also be merged with the Marchand-balun to increase the co-designed bandwidth [15]. The dipoles were printed on vertical bricks with each brick made up of two dielectric layers that carry the balun and antenna elements. The inter-element capacitance of the TCDA was implemented using the overlap between those layers among the adjacent elements. However, the design features provided by Doane et al. [15] become too small and beyond the PCB-fabrication capabilities at Ka band. Multi-layer design is extremely difficult to implement; therefore, achieving the desired inter-element capacitance is raised as a concern.

In Fig. 3, a unit cell model of tightly coupled dipole array at Ka-band using a single dielectric-layer is presented. The separation between the dipole tips of the adjacent cells is used to achieve the inter-element capacitance. The closest possible separation is 80 m tip-to-tip, and it is governed by the fabrication capabilities of the PCB technique. Consequently, the maximum bandwidth that can be achieved in this case is  $\approx 2.2 : 1$ .

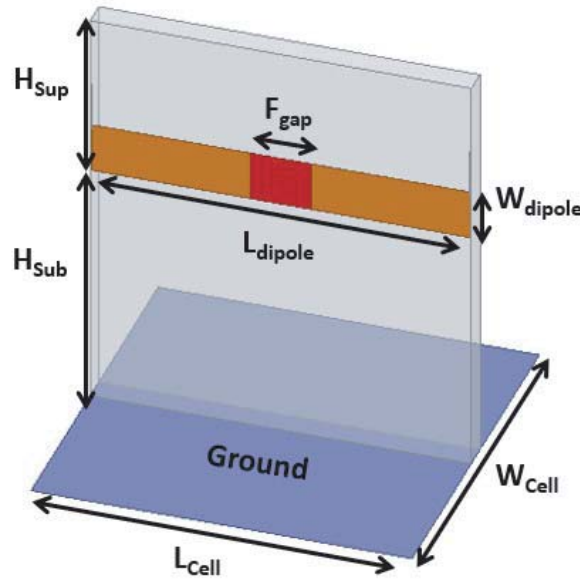


**Figure 3.** Initial design of the tightly coupled dipole array unit cell at Ka-band.  $L_{cell} = W_{cell} = 3.75$  mm,  $L_{dipole} = 3.67$  mm,  $W_{dipole} = 0.5$  mm,  $H_{sub} = 2.5$  mm,  $F_{gap} = 0.6$  mm.

The circuit model of the TCDA unit cell, as proposed by [25], is shown in Fig. 4(a). It consists of the following design specifications:  $Z_o = 377$ ,  $Z_{sup} = Z_{sub} = 238$ ,  $C_{coupling} = 0.5$  pF,  $L_{dipole} = 0.6$  nH. This model treats the dipole as a short wire with the gap at the feeding points ( $F_{gap}$ ) neglected. On the other hand, Fig. 5(a) shows that the gap at the feeding points ( $F_{gap}$ ) has significant effect on the input impedance of the unit cell considering its inductive behavior at the upper frequency band and capacitive behavior at the lower band. This property can be utilized to improve the impedance bandwidth of the 3D model to 2.6 : 1 as shown in Fig. 5(b). In Fig. 4(b), the feed gap as an inductance ( $L_{feed}$ ) in parallel with a capacitance ( $C_{feed}$ ) related proportionally to the gap separation is proposed [26]. This provides a more accurate circuit model in consideration with the effect of the feed gap. The new circuit model

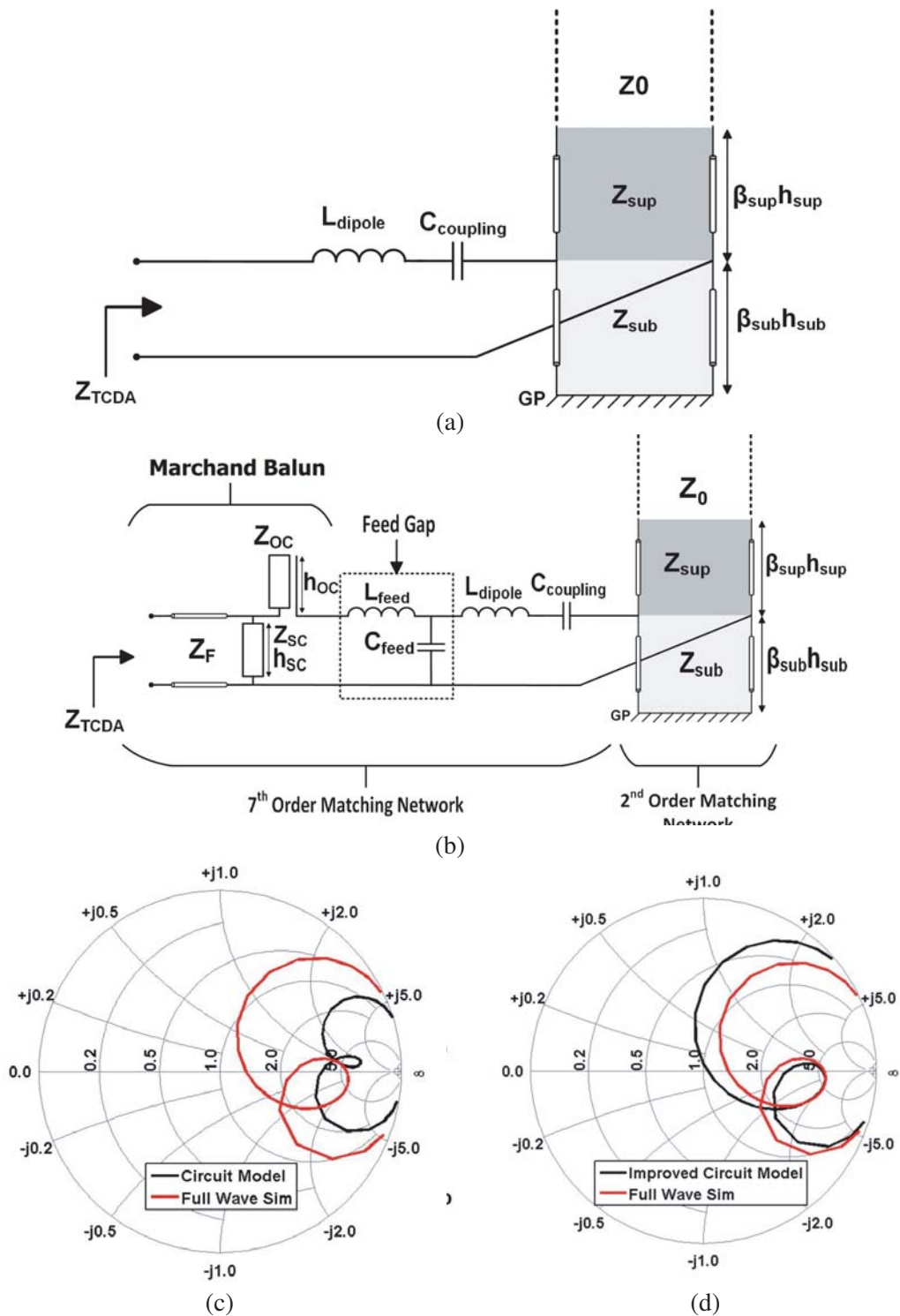


**Figure 4.** (a) Equivalent circuit of tightly coupled dipole array as proposed in [25]. (b) Proposed improved equivalent circuit of the tightly-coupled dipole array with integrated balun. (c) Smith plot of input impedance obtained from circuit model of [25] and (d) the proposed improved model of this work, compared to the full wave simulation.

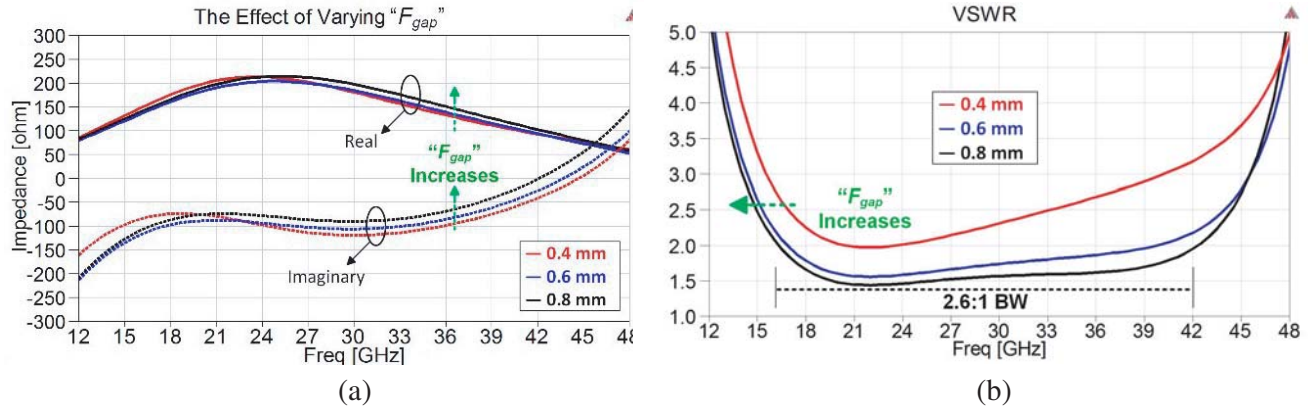


**Figure 5.** The effect of changing  $F_{gap}$  on the; (a) Input impedance of the unit cell, (b) VSWR.

is tuned with the simulated results of the 3D model and achieved  $C_{feed} = 0.06$  pF and  $L_{feed} = 0.4$  nH. As shown in Figs. 4(c) and (d), a better match between the circuit model and the 3D full wave model is reached after adding the ( $F_{gap}$ ) effect. There is a limit on how much feed gap separation can be increased. Increasing ( $F_{gap}$ ) beyond a certain limit creates higher order modes and ( $C_{feed}$ ) becomes almost negligible.

The final unit cell design of the proposed TCDA at Ka-band is shown in Fig. 6. The dipoles are printed on a single-side of the substrate. As the element feed, a planar Marchand-balun [15, 27] compatible with the surface-mount phase shifter is integrated between the ground and the radiating aperture. The phase shifter is represented by a  $1.8 \text{ mm} \times 1.8 \text{ mm}$  silicon box at the back side of the unit cell with its ground plane added as well. The antenna and the feed are tuned, using the new circuit model, shown in Fig. 4(b), to achieve optimum impedance behavior over the entire band of interest (10–40 GHz) with the following specifications:  $Z_{OC} = 25 \Omega$ ,  $h_{OC} = 1.1 \text{ mm}$ ,  $Z_{SC} = 165 \Omega$ ,  $h_{SC} = 1 \text{ mm}$ ,  $Z_F = 75 \Omega$ ,  $Z_{TCDA} = 75 \Omega$ . The 3D model is then reoptimized by printing the dipole antenna element and the feeding structure on a vertically-placed low-loss Rogers 3010 ( $\epsilon_r = 10.2$ ) substrate [15]. The proposed array topology is designed using Ansoft HFSS v.15 and an impedance bandwidth of 13–42 GHz with VSWR < 2.5 is achieved in an infinite array setting, for up to a  $45^\circ$  scan angle, as shown in Fig. 6(b). The beam scan performance is further evaluated by simulating a finite  $8 \times 8$  sub-array, as discussed below.

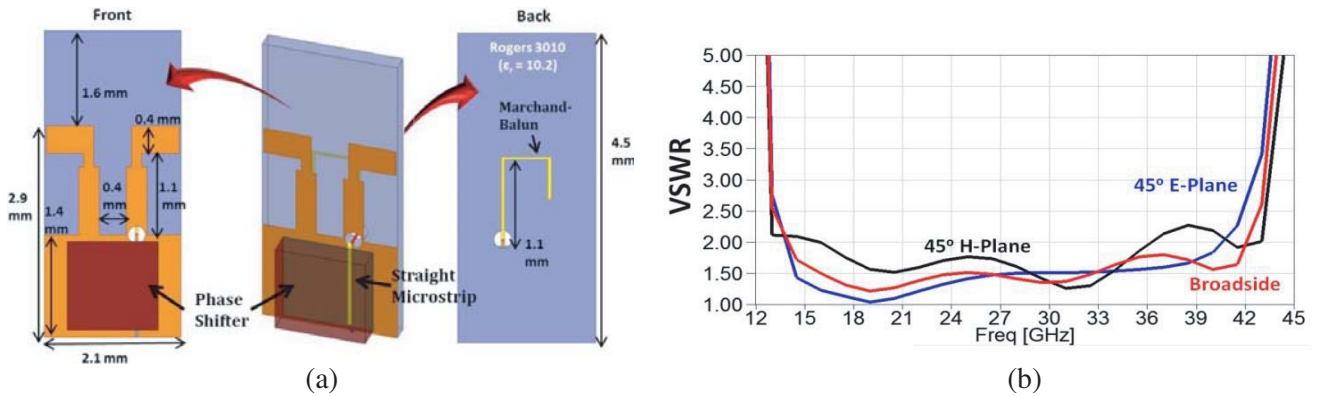


**Figure 6.** Marchand-balun fed, TCDA unit cell with integrated MEMS phase shifter; (a) Unit cell design and (b) computed active VSWR.

#### 4. CHARACTERIZATION AND MEASUREMENTS OF THE FINITE TCDA PROTOTYPE

Most of the work in the previous section is based on the unit cell design. The unit cell represents the performance of an infinite array. However, in reality, infinite array cannot be achieved. It has to be truncated to a limited number of elements which is found to increase the reflection at the feeding ports, due to what is called surface waves. Surface waves travel back and forth at the aperture of the array, and alter the induced voltages at the elements, leading to variations in the active impedance values and impedance mismatch. Several techniques were proposed to solve the issue including taper excitation and most importantly, the characteristic mode excitation [36]. This technique is based on nonuniform excitation of the elements to compensate for the induced voltages that are added by the surface waves to achieve a better match. The characteristic mode excitation are applied and found to give perfect matching for array elements, leading to high efficiency [37]. However, the main drawback of this technique is that it requires a custom-made feeding network. Surface waves on their way back from the edges to the center elements can be weakened by edge element termination. This technique utilizes short circuit, open circuit, resistors, or a combination of them at the edges to eliminate the surface waves.

An  $8 \times 8$ -element dipole array prototype was simulated for the optimum termination type, and the number of terminated elements based on VSWR, and radiation efficiency are shown in Fig. 7. It is found that the optimum number of dummy elements at each side should be around 50% of array size [28]. Hence, for an 8-elements array, four dummy elements at each side would give the lowest VSWR using the lowest array size. Furthermore, dummy elements terminated with a short circuit are determined to offer higher efficiency than resistively terminated elements, and wider bandwidth than open-circuited ones, as shown in Fig. 7(b).

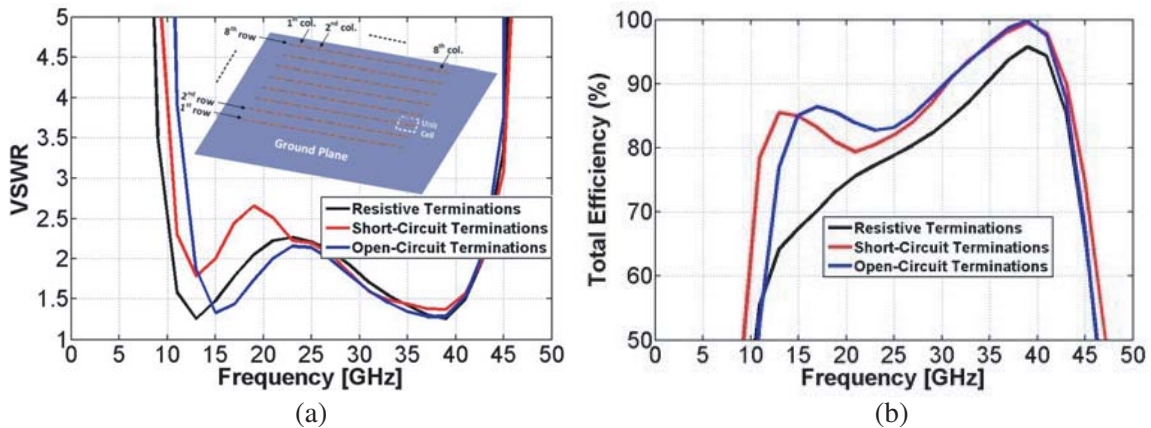


**Figure 7.** Comparison between resistive, short-circuit and open-circuit termination of an  $8 \times 8$  TCDA aperture. (a) VSWR, and (b) total efficiency.

To examine the beam scan performance, an  $8 \times 8$ -element, single polarization TCDA prototype was designed as shown in Fig. 8. The array is fed using lumped port at each element, and phase signal is delivered to each port for a certain beam angle up to  $\theta = \pm 45^\circ$  with  $15^\circ$  step. Fig. 8 shows beams scan performance at various frequencies in  $E$ - and  $H$ -plane. The beam is examined at three different frequencies to fully cover the operational bandwidth. It is observed that the beam scan performance is achieved in both the  $E$ -plane and the  $H$ -plane, with sidelobe level (SLL) below  $-10$  dB and cross polarization levels better than  $-10$  dB. The pattern in  $H$ -plane is smoother than  $E$ -plane pattern, which is referred to the surface waves at  $E$ -plane. Although edge termination is added to the array to reduce the surface waves, in reality, it is difficult to entirely eliminated them.

A simplified low cost,  $4 \times 4$  version was fabricated to validate the proposed design. The array is fed by a 4 : 1 power divider on the same brick, as shown in Fig. 9. The divider consists of T-Junction power

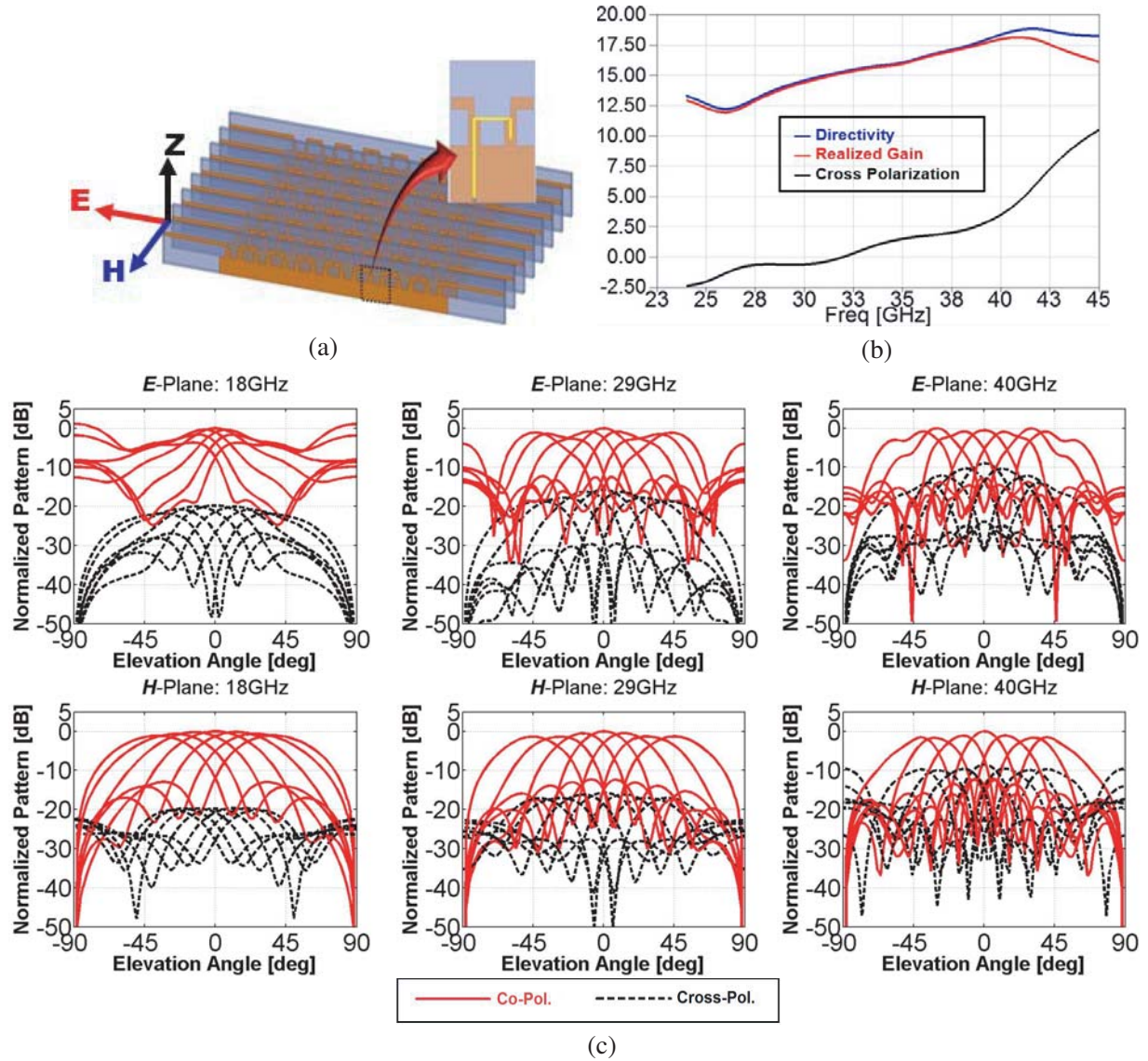


**Figure 8.** Performance of the  $8 \times 8$  array. (a) Array structure, (b) broadside realized gain, and (c) beam scan performance at different frequencies.

dividers backed by a Wilkinson divider to achieve low loss while having a good isolation between the input ports. The Wilkinson divider in this design utilizes a  $100\ \Omega$  lumped impedance. Each row of the  $4 \times 4$  array was fabricated on printed circuit board and assembled as shown in Fig. 10(a). Subsequently, the prototype was mounted on a metal platform that supports the 4 : 1 Wilkinson power divider, as shown in Fig. 10(b). The power divider and the array are connected through high frequency coaxial cables with phase match  $< 1$  ps (better than  $15^\circ$  at 40 GHz) to guarantee minimal phase difference at all elements.

Measurements from the simulation are obtained through the compact range anechoic chamber at the Ohio State University ElectroScience Laboratory. The effects of path loss and feed cables are factored out from the measurements of the antenna under test (AUT) using a standard gain calibration antenna. The reflection coefficient is determined at the output of each PCB layer which is then used to calculate the corporate VSWR. For simplicity, the corporate network assumes 1 :  $N$  divider/combiner that is lossless, perfectly matched at all ports, with perfect phase balance and infinite isolation between the output ports.

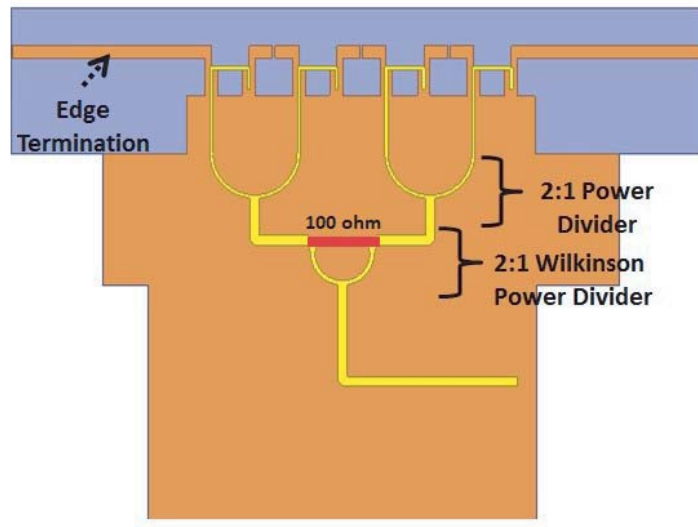


**Figure 9.** A Single brick of the proposed  $4 \times 4$  element TCDA with feeding network.

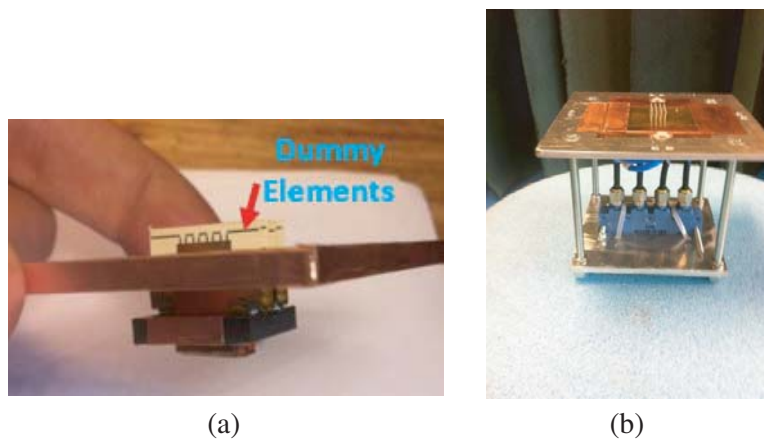


**Figure 10.** The fabricated  $4 \times 4$  design. (a) The array assembly including the feeding network. (b) Array on a metal platform fed by a 4 : 1 power divider.

As shown in Fig. 11, the  $4 \times 4$  array supports a measured impedance bandwidth of 18–40 GHz at  $VSWR < 2$ . Fig. 12 compares the measured and simulated broadside gains of the fabricated  $4 \times 4$  array and presents radiation pattern at selected frequencies in  $E$ - and  $H$ -planes. As shown, the measured patterns match the simulations, and the array has  $\approx 8$  dB of realized gain at 38 GHz. The pattern at 28 GHz shows some ripple at broadside direction, as well as the realized gain dips at certain frequencies, due to finite size effects stemming from the small number of array elements that are used. This dip has been resolved by increasing the number of elements in the simulation to  $8 \times 8$ , see Fig. 8(b). Absorbers can also be used at the edges of the array to eliminate the edge effect.

## 5. AN 18–30 GHz TWO-BIT TUNABLE SWITCHED NETWORK MEMS PHASE SHIFTER

As discussed in Section 2, accurate beam steering requires a corporate feeding network that guarantees equi-phase currents and unsquinted beam over the entire band. Corporate networks require phase delay units for beam steering. While true time delay units are ideal for wideband applications, they are lossy and bulky. Hence, a low-loss compact solid-state phase shifter that can be used at the unit

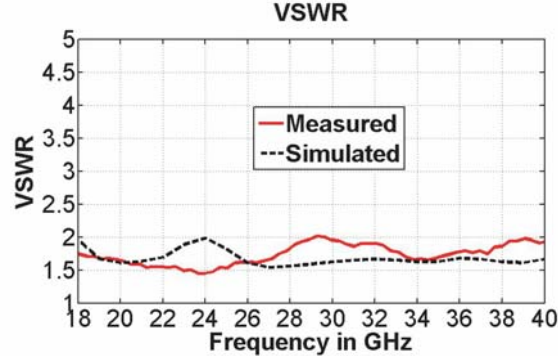


**Figure 11.** Measured and computed broadside performance of the  $4 \times 4$  TCDA prototype.

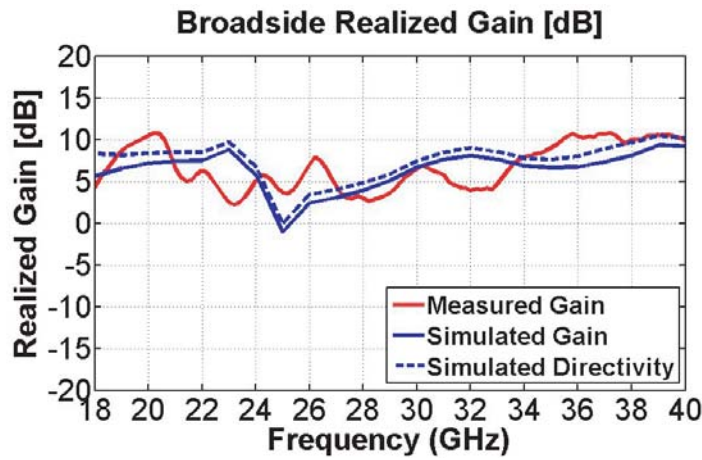
cell of moderate bandwidth arrays of 18–30 GHz is proposed. The size of the phase shifter is below  $1.8 \text{ mm} \times 1.8 \text{ mm}$  to allow seamless integration with the proposed TCDA design.

Solid-state phase shifters are compatible with microwave components in terms of shape. They also consume less DC power than ferrite and also provide lower losses. Hence, they can be seamlessly integrated into the proposed design to reduce the assembly cost of the phase array system [29]. Solid-state phase shifters that utilize micro-electro mechanical system (MEMS) technology in their design show lower loss and more compactness, especially, at high frequencies 8–100 GHz [30–32]. Additionally, MEMS switches have very small up-state capacitance that results in wideband performance over similar designs using FET or PIN devices. The up-state capacitance in RF MEMS capacitive shunt switches is formed between the thin metallic bridge, anchored at both ground conductors of the CPW, and the central signal line. This capacitance is very small (10–100 fF) and does not affect the impedance of the signal line. Thus, the switch simply acts as an ON-state causing RF signal to pass through the transmission line from one end to another end.

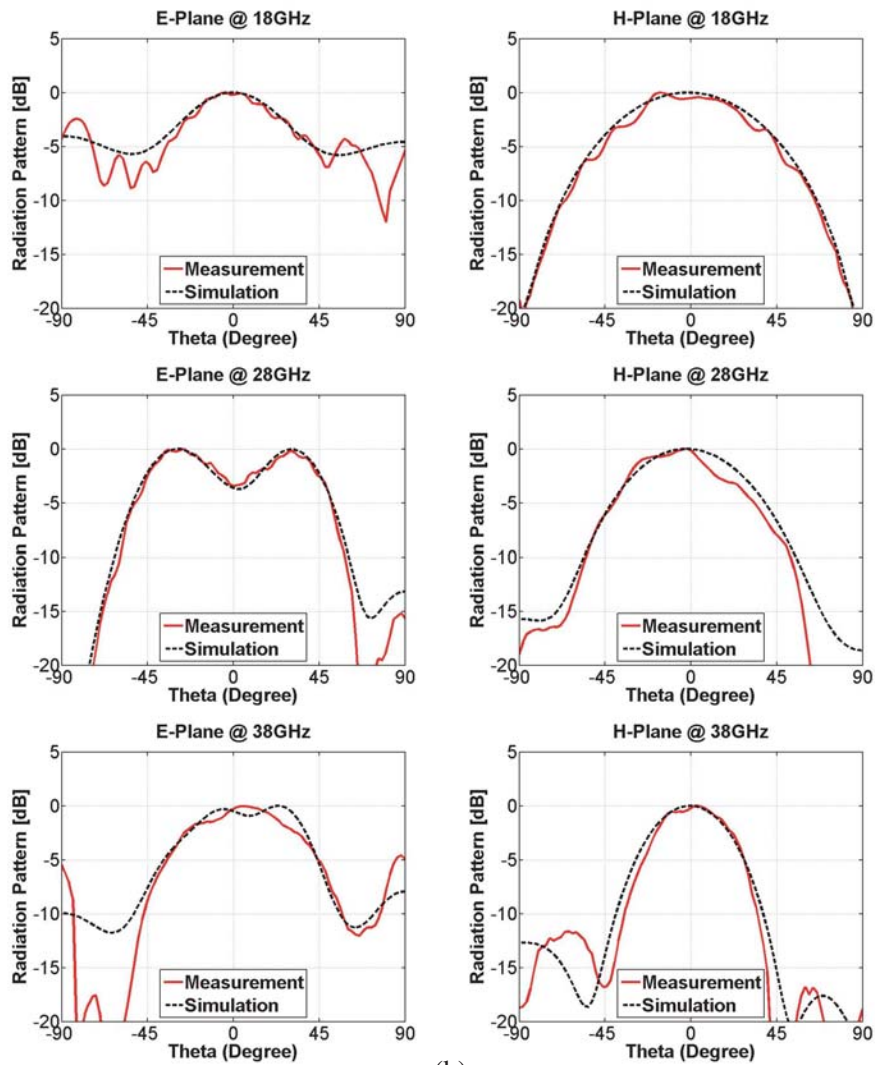
The proposed phase shifter topology is developed using a switched network design, shown in Fig. 13. Solid-state phase shifters can exist with different topologies such as reflector type, switched line, loaded-line, and phase shifters which are based on switched network [29]. A common phase shifter design based on switch networks results in a much smaller form factor than the switched line type. Moreover, such architectures have gained popularity at the range 6–35 GHz [33–35]. Switched network phase shifter typically uses the low-pass/high-pass filter topology. In this topology, the low-pass results in phase delays, whereas, the high-pass results in phase advance. Fig. 13 shows a two-bit switched network phase shifter based on this design. It is initially tuned using the circuit model in order to achieve the following delays:  $-135^\circ$ ,  $-45^\circ$ ,  $45^\circ$  and  $135^\circ$ , where;  $C_1 = C_2 = 0.088 \text{ pF}$ ,  $C_3 = 0.214 \text{ pF}$ ,  $C_4 = 0.037 \text{ pF}$ ,  $L_1 = L_2 = 0.5 \text{ nH}$ ,  $L_3 = 0.7 \text{ nH}$ , and  $L_4 = 0.35 \text{ nH}$ .

The design is then implemented using a full wave simulator utilizing MEM switches for network selection. Tunable MEMS capacitances are used with planar coil inductors. The diameter and number of turns of the planar inductor are determined based on the study by Taniguchi et al. [35]. The simulation performance is curve fitted with the circuit model to obtain the optimum value of the capacitors per filter network design. Fig. 14 shows the 3D model of the  $180^\circ$  LPF network as an example. The enter frequency of the band is optimized through tunable MEMS capacitors, with a planer ring inductor added in parallel. The simulated performance shown in (b) demonstrates well behaved response and high match with the circuit model. Fig. 15 also presents the proposed two-bit tunable switched network MEMS phase shifter.

For finer delays, tunable capacitors are utilized to enable continuous coverage up to  $360^\circ$  and bandwidth tuning. The entire circuit is built on a high resistivity silicon layer with  $\epsilon_r = 11.9$ . Planar coil inductors and MEMS capacitors are also used for compactness. The dimensions of each phase shifter are  $1.8 \text{ mm} \times 1.8 \text{ mm} \times 0.3 \text{ mm}$ , whereas the separation between the input and output (RF IN and RF OUT) is 1.3 mm. As shown in Figs. 15(b) and (c), linear phase shift versus frequency is achieved in both  $180^\circ$  and  $90^\circ$  phase delay networks respectively. The  $180^\circ$  switched network consists of LPF network with  $-90^\circ$  phase delay at the center frequency, and HPF network with  $+90^\circ$  phase advance at the center frequency. Similarly, the  $90^\circ$  switched network consists of LPF network with  $-45^\circ$  phase



(a)



(b)

**Figure 12.** Measured and computed broadside performance of the  $4 \times 4$  Ka-band TCDA prototype: (a) realized gain, and (b) radiation pattern.

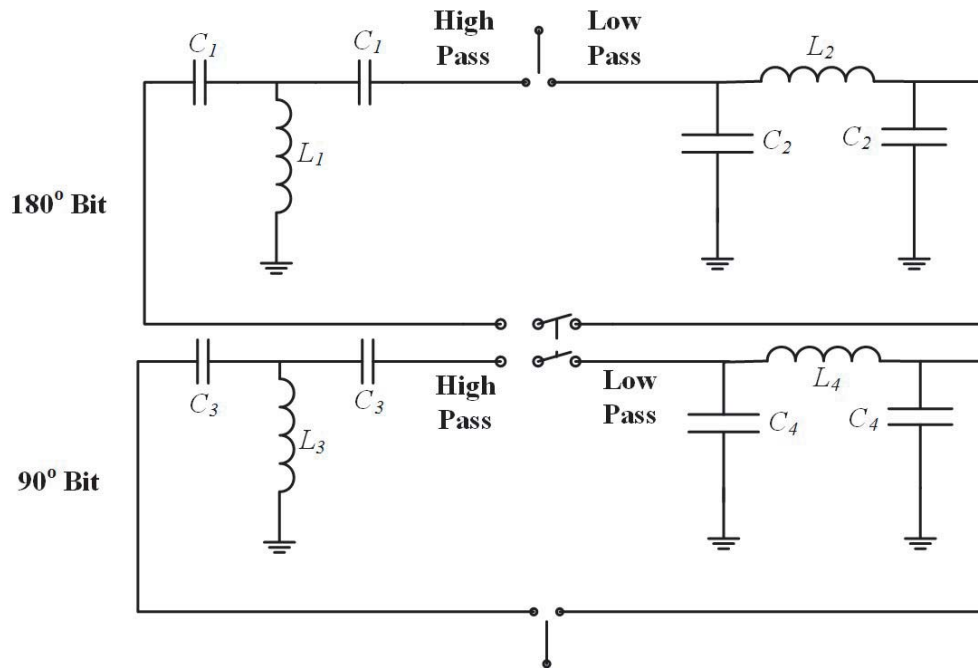


Figure 13. two-bits switched network phase shifter using high-pass/low-pass filter configurations.

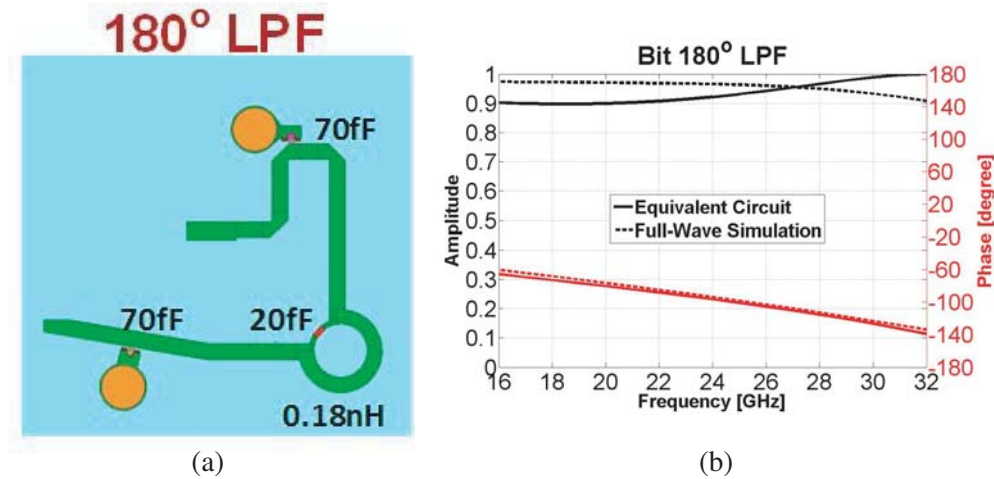
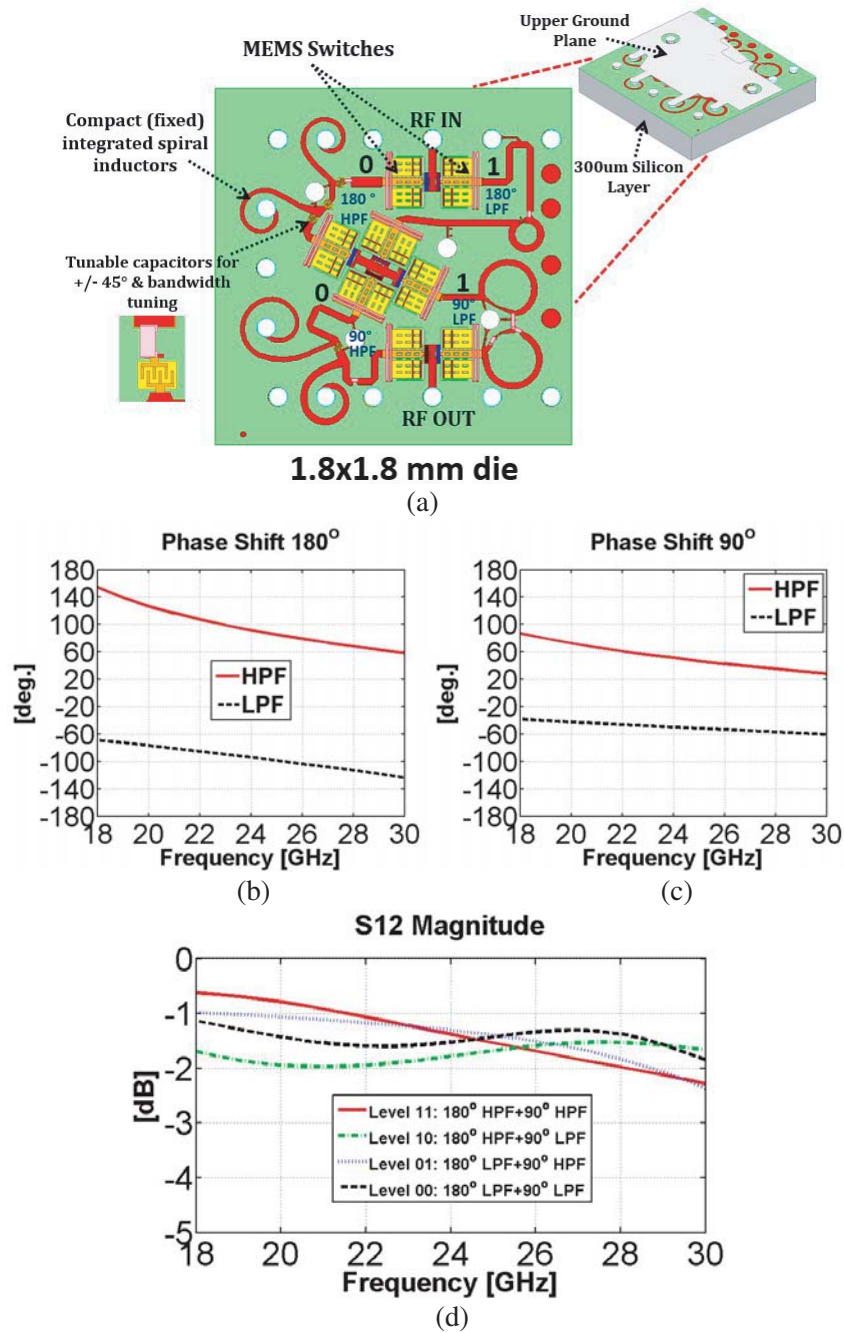


Figure 14. (a) 3D model of 180° LPF network design. (b) Simulated performance compared with the circuit model.

delay and HPF with +45° phase advance. The insertion loss of the phase shifter for all possible signal paths as shown in (d). They are denoted as level 11, which consists of HPF network of the 180° bit and HPF network of the 90° bit; level 10 consisting of HPF network of the 180° bit and LPF network of the 90° bit; level 01 that consists of LPF network of the 180° bit and HPF network of the 90° bit; and level 00 that consists of LPF network of the 180° bit and LPF network of the 90° bit. Overall, the phase shifter provides continuous phase shift over the band 18–30 GHz and < 2.5 dB insertion loss as shown in (d). The compact form of the phase shifter allows for the integration into array elements of the TCDA design as described earlier.



**Figure 15.** (a) Low-profile two bits MEMS phase shifter based on switched low-pass/high-pass networks design and MEMS switches, (b) corresponding phase delay performance of HPF/LPF 180° network, (c) corresponding phase delay performance of HPF/LPF 90° network and (d) insertion loss in [dB].

## 6. BEAM STEERING WITH MEMS PHASE SHIFTERS

In this section, the beam scan performance of the proposed beam former is examined using the actual MEMS phase shifters integrated with the TCDA array design. The coupling level and the VSWR are all affected by scanning. Accordingly, 4× infinite prototype of the array is designed and simulated on ANSYS HFSS v.15. Each element in the array is integrated with the corresponding phase shifter track to scan at 45° as shown in Fig. 16. Due to the complexity of the MEMS phase shifter, only one scan

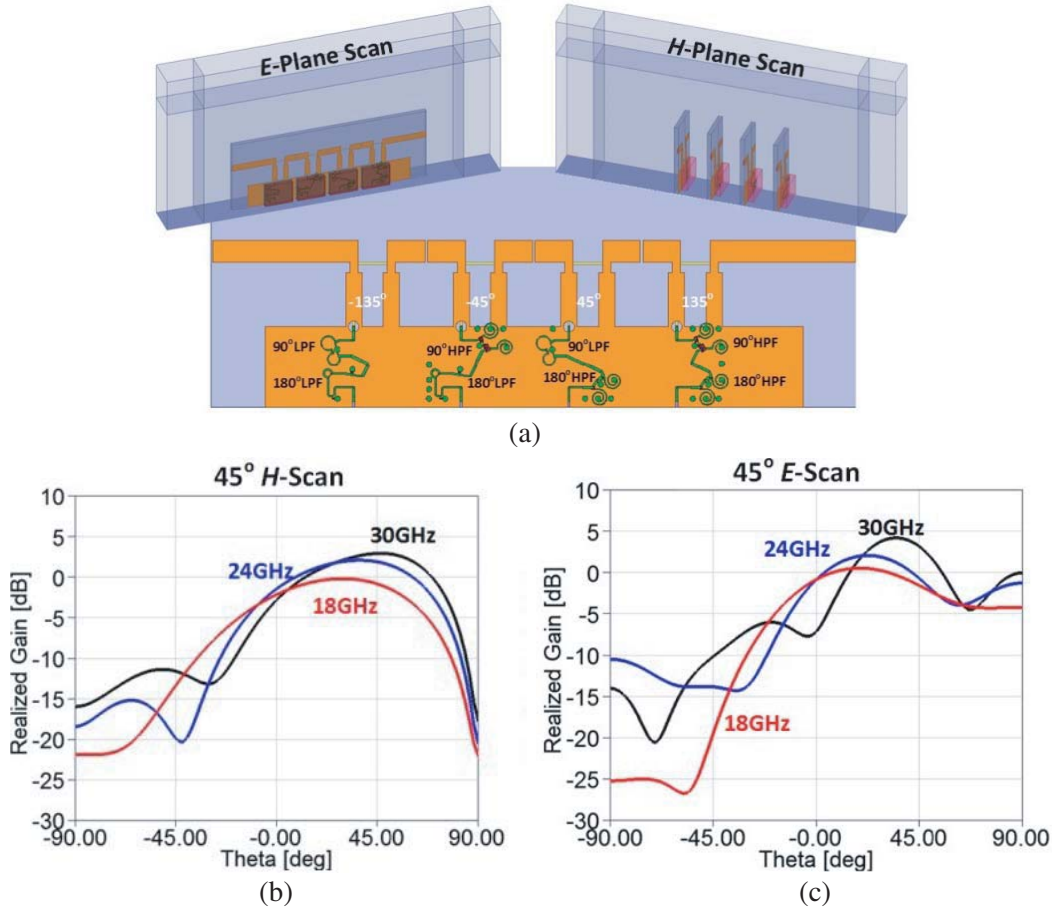


**Figure 16.** (a) CDA with Integrated MEMS phase shifters that are tuned at 45° scan. (b) Realized gain in  $H$ -plane, and (c) realized gain in  $E$ -plane.

angle, i.e., 45°, was selected for illustrating the performance. Radiation pattern is plotted at three different frequencies as shown, and the beam is successfully scanned to 45° at SLL < -10 dB with no squint observed.

Beam steering to different scan angles can be achieved by selecting different propagating signal networks in the phase shifters. The designed phase shifter consists of 4 networks (2 bits). The total phase shift is determined by the RF path length of the selected networks. The selection between the different networks is controlled using RF-MEMS ohmic switches monolithically integrated into the network, as given in Fig. 15(a). Once the MEMS switches are actuated, the RF signal travels through the selected network and the radiating beam is steered by a predefined value.

## 7. CONCLUSION

A beam steering model consisting of tightly-coupled dipole array and RF-corporate feeding network is developed for SATCOM applications at 18–40 GHz. The array is designed based on a simple, single layered structure for affordable PCB fabrication cost. The simulated performance of an 8 × 8 array shows that it is capable of scans to  $\theta = 45^\circ$  in the  $E$ -, and  $H$ -planes at SLL < -10 dB over 18–40 GHz. A proof-of-concept 4 × 4 array is fabricated using off-the-shelf Rogers 3010 substrates and is characterized for broadside scan. The measurements demonstrate promising gain over entire bandwidth. For beam forming, a novel feeding architecture for moderate bandwidth, 18–30 GHz, large arrays is proposed. For corporate network with phase shifter adapted at each element, a low-Solid-state MEMS phase shifter is developed for beam forming providing advantages such as compactness and low-loss. The phase shifter is integrated at the backside of each unit cell element leading to further reduce the loss, size,

and complexity of the array-feeding network. A reliable full-wave simulation of the entire beam forming system, consisting of array/feed and actual MEMS phase shifter, is demonstrated over 18–30 GHz band in both  $E$ - and  $H$ -planes.

## REFERENCES

1. Abumunshar, A. J., N. K. Nahar, D. Hyman, and K. Sertel, "18–40 GHz low-profile phased array with integrated MEMS phase shifters," *EuCAP*, Paris, France, March 2017.
2. Abumunshar, A. J., N. K. Nahar, D. Hyman, and K. Sertel, "K-to-Ka band low-profile phased array with integrated MEMS phase shifters," *IEEE International Symposium on Antennas and Propagation and National Radio Science Meeting (USNC/URSI 2016)*, Fajardo, BR, July 2016.
3. Gargione, F., T. Iida, F. Valdoni, and F. Vatalaro, "Services, technologies, and systems at Ka band and beyond — A survey," *IEEE Journal on Selected Areas in Communications*, Vol. 17, No. 2, 133–144, 1999.
4. Trunk, G., et al., "Advanced multifunction RF system (AMRFS) preliminary design considerations," *NRL*, Washington, DC, December 2001.
5. Tavik, G. C., J. Y. Choe, and P. K. Hughes, "Advanced Multifunction Radio Frequency (AMFR) concept testbed overview," *Government Microcircuit Application Conf. Dig.*, March 2001.
6. Foshee, J., R. Tahim, and K. Chang, "A High capacity phased array antennas for theater recce/intel networks," *IEEE Aerospace Conference Proceedings*, Vol. 2, 841–853, 2002.
7. Krauss, A., H. Bayer, R. Stephan, and M. Hein, "Low-profile tracking antenna for Ka-band satellite communications," *IEEE — APS Topical Conference on (APWC)*, Torino, 2013.
8. Grajek, P. R., B. Schoenlinner, and G. M. Rebeiz, "A 24-GHz high-gain Yagi-Uda antenna array," *IEEE Transactions on Antennas and Propagation*, Vol. 52, No. 5, 1257–1261, May 2004.
9. Gheethan, A. A., M. C. Jo, and G. Mumcu, "Microfluidic based Ka-band beam-scanning focal plane array," *IEEE Antennas and Wireless Propagation Letters*, Vol. 12, 1638–1641, 2013.
10. Encinar, J., M. Barba, J. Page, M. Arrebola, A. Pacheco, and K. van't Klooster, "Experimental validation of a reflect array antenna in Ka-band," *IEEE International Symposium on Antennas and Propagation (APSURSI)*, 353–356, Spokane, WA, 2011.
11. Munk, B. A., *Finite Antenna Arrays and FSS*, Ch. 6, 181–213, Piscataway, IEEE Press/Wiley-Interscience, 2003.
12. Zhou, Y., et al., "Tightly coupled array antennas for ultra-wideband wireless systems," *IEEE Access*, Vol. 6, 61851–61866, 2018.
13. Moulder, W., K. Sertel, and J. Volakis, "Superstrate-enhanced ultrawideband tightly coupled array with resistive FSS," *IEEE Transactions on Antennas and Propagation*, Vol. 60, No. 9, 4166–4172, September 2012.
14. Shim, J., J. Go, and J. Chung, "A 1-D tightly coupled dipole array for broadband mmwave communication," *IEEE Access*, Vol. 7, 8258–8265, 2019.
15. Doane, J. P., K. Sertel, and J. L. Volakis, "A wideband, wide scanning Tightly Coupled Dipole Array with Integrated Balun (TCDA-IB)," *IEEE Trans. on Antennas and Propagation*, Vol. 61, No. 9, 4538–4548, September 2013.
16. Agrawal, A. K. and E. L. Holzman, "Beamformer architectures for active phased-array radar antennas," *IEEE Transactions on Antennas and Propagation*, Vol. 47, No. 3, 432–442, 1999.
17. Vinoy, K. J. and V. K. Varadan, "Design of reconfigurable fractal antennas and RF-MEMS for space-based systems," *Smart Materials and Structures*, Vol. 10, No. 6, 2001.
18. Ruffin, P. B., J. C. Holt, J. H. Mullins, T. Hudson, and J. Rock, "MEMS-based phased arrays for army applications," *The 14th International Symposium on: Smart Structures and Materials & Nondestructive Evaluation and Health Monitoring*, 652802–652802, International Society for Optics and Photonics, 2007.

19. Malmqvist, R., C. Samuelsson, B. Carlegrim, P. RantaKari, T. Vaha-Heikkila, A. Rydberg, and J. Varis, "Ka-band RF MEMS phase shifters for energy starved millimetre-wave radar sensors," *Semiconductor Conference (CAS)*, Sinaia, 2010.
20. Corey, L., E. JasKa, and J. Guerci, "Phased-array development at DARPA," *IEEE International Symposium on Phased Array Systems and Technology*, 2003.
21. Munk, B. A., *Finite Antenna Arrays and FSS*, Wiley, New York, 2003.
22. Tzanidis, I., C. C. Chen, and J. L. Volakis, "Low profile spiral on a thin ferrite ground plane for 220–500 MHz operation," *IEEE Transactions on Antennas and Propagation*, Vol. 58, No. 11, 3715–3720, November 2010.
23. Yetisir, E., N. Ghalichechian, and J. L. Volakis, "Ultrawideband array with 70° scanning using FSS superstrate," *IEEE Transactions on Antennas and Propagation*, Vol. 64, No. 10, 4256–4265, October 2016.
24. Novak, M. H., J. L. Volakis, and F. A. Miranda, "Wideband array for C, X, and Ku-band applications with 5.3 : 1 bandwidth," *IEEE International Symposium on Antennas and Propagation & USNC/URSI National Radio Science Meeting*, Vancouver, BC, 2015.
25. Munk, B. A., "Broadband wire arrays," *Finite Antenna Arrays and FSS*, 181–213, 1st Edition, Wiley-IEEE Press, July 2003.
26. Alwan, E. A., K. Sertel, and J. L. Volakis, "Circuit model based optimization of ultra-wideband arrays," *Proceedings of the 2012 IEEE International Symposium on Antennas and Propagation*, Chicago, IL, 2012.
27. Doane, J., K. Sertel, and J. Volakis, "A 6.3 : 1 bandwidth scanning tightly coupled dipole array with co-designed compact balun," *Antennas and Propagation Society International Symposium (APSURSI)*, Chicago, IL, 2012.
28. Abumunshar, A. J., "Simulated finite array performance," *Tightly Coupled Dipole Array with Integrated Phase Shifters for Millimeter-Wave Connectivity: Simulated Finite Array performance*, 119–129, OhioLINK Electronic Theses and Dissertations Center, Electronic Thesis or Dissertation. Ohio State University, May 2017.
29. Rebeiz, G. M., *MEMs phase shifters, in, RF MEMS: Theory, design, and technology*, 259–259, John Wiley and Sons, Inc., Hoboken, New Jersey, 2003.
30. Yamini, A. and M. Soleimani, "Multiband behavior of wideband Sierpinski fractal bow-tie antenna," *The European Conference on Wireless Technology*, Paris, 2005.
31. Lu, Y. J., Y. W. Liu, and P. Hsu, "A hybrid design of printed antenna fed by coplanar waveguide with and without back conductor," *IEEE Antennas and Wireless Propagation Letters*, Vol. 13, 1597–1600, 2014.
32. Li, R., B. Pan, T. Wu, K. Lim, J. LasKar, and M. Tentzeris, "A broadband printed dipole and a printed array for base station applications," *Antennas and Propagation Society International Symposium*, San Diego, CA, 2008.
33. Wallace, J., H. Redd, and R. Furlow, "Low cost MMIC DBS chip sets for phased array applications," *IEEE MTT-S International Microwave Symposium Digest (Cat. No.99CH36282)*, Vol. 2, 677–680, Anaheim, CA, USA, 1999.
34. Campbell, C. F. and S. A. Brown, "A compact 5-bit phase-shifter MMIC for K-band satellite communication systems," *IEEE Transactions on Microwave Theory and Techniques*, Vol. 48, No. 12, 2652–2656, December 2000.
35. Taniguchi, E., M. Hieda, H. Kurusu, M. Funada, Y. Iyama, and T. Takagi, "A Ku-band matched embedded-FET phase shifter," *29th European Microwave Conference*, 357–360, Munich, Germany, 1999.
36. Garbacz, R. and R. Turpin, "A generalized expansion for radiated and scattered fields," *IEEE Transactions on Antennas and Propagation*, Vol. 19, No. 3, 348–358, May 1971.
37. Tzanidis, I., "Ultrawideband low-profile arrays of tightly coupled antenna elements: Excitation, termination and feeding methods," Ph.D. Dissertation, The Ohio State University, 2011.